



Published in final edited form as:

J Pharm Sci. 2018 September ; 107(9): 2325–2334. doi:10.1016/j.xphs.2018.05.019.

Effect of Two Emulsion-Based Adjuvants on the Structure and Thermal Stability of *S. aureus* Alpha-toxin

Yangjie Wei¹, Jian Xiong¹, Nicholas R. Larson¹, Vidyashankara Iyer², Gautam Sanyal², Sangeeta B. Joshi¹, David B. Volkin¹, and C. Russell Middaugh^{1,*}

¹Macromolecule and Vaccine Stabilization Center, Department of Pharmaceutical Chemistry, University of Kansas, 2030 Becker Drive, Lawrence, Kansas 66047, USA

²Biopharmaceutical Development, Medimmune Inc., Gaithersburg, Maryland 20878, USA

Abstract

The effects of two squalene based emulsion adjuvant systems (ME.0 and SE) on the structure and stability of the recombinant protein antigen alpha-toxin (AT), a potential vaccine candidate for *Staphylococcus aureus* infection, were investigated using Fourier Transform Infrared (FTIR) and both steady-state and time-resolved intrinsic fluorescence spectroscopy as well as differential scanning calorimetry (DSC). A component study, performed to identify the effects of the individual emulsion's components, showed negligible interactions between AT and ME.0. DSC analysis showed the ME.0 emulsion thermally destabilized AT, probably because of changes in the buffer composition of AT upon mixing. The SE emulsion caused increased alpha-helix and decreased beta-sheet content in AT, and a significant blue shift in the fluorescence spectra relative to that of AT in solution. DSC analysis showed SE exerted a dramatic thermal stabilization effect on AT, probably attributable to an interaction between AT and SE. Size exclusion chromatography showed a complete loss in the recovery of AT when mixed with SE, but not ME.0, indicating a high degree of interaction with SE. This work successfully characterized the biophysical properties of AT in the presence of two emulsion adjuvants including a component study to rationalize how emulsion components affect protein antigen stability.

Keywords

Staphylococcus aureus alpha-toxin; emulsion adjuvant; vaccine formulation; squalene; stability; protein structure

Introduction

Subunit vaccines contain defined macromolecular components identified from a pathogen that are capable of eliciting protective immunity.¹ They are usually recombinant proteins and

*Correspondence to: C. Russell Middaugh, Department of Pharmaceutical Chemistry, 2030 Becker Dr., University of Kansas, Lawrence, KS 66047. middaugh@ku.edu; Telephone: +785-864-5813; Fax: +785-864-5814.

Publisher's Disclaimer: This is a PDF file of an unedited manuscript that has been accepted for publication. As a service to our customers we are providing this early version of the manuscript. The manuscript will undergo copyediting, typesetting, and review of the resulting proof before it is published in its final citable form. Please note that during the production process errors may be discovered which could affect the content, and all legal disclaimers that apply to the journal pertain.

possess many advantages over other vaccine types (e.g. live attenuated and inactivated viruses and bacteria) such as an improved safety profile, a highly defined nature, ease of production and potential for lower cost of goods.^{1; 2} One important limitation of subunit vaccines is that they usually induce relatively weak immunogenicity owing to their inability to replicate and/or lack of other immunostimulatory components such as pathogen-associated molecular pattern molecules to induce innate and cellular immunity.³ To ensure the successful immunization of subunit vaccines, they are often administered with adjuvants to boost host immune responses.³

Oil-in-water (O/W) emulsion-based adjuvants are an important class of adjuvants used for subunit vaccines.⁴⁻⁶ These emulsions usually use squalene as the oil phase, which is a naturally occurring lipid found in plants, animals and humans. Suitable surfactants (e.g., Tween 80, Span 85 etc.) are used to stabilize oil droplets dispersed in the aqueous environment. Currently, two squalene-based emulsion adjuvants (MF59 and AS03) have been approved for commercial use.⁷⁻⁹ Potent immunopotentiators, such as monophosphoryl lipid A (MPLA), can be added to emulsion-based adjuvants to further improve their adjuvanticity. For example, a squalene emulsion containing a Glucopyranosyl Lipid Adjuvant (GLA), a synthetic form of MPLA, is currently used in a phase II trial for a respiratory syncytial virus vaccine.^{10; 11} In this work, MedImmune emulsion. 0 (ME.0) and Stable Emulsion (SE) O/W emulsions were investigated. Both contain squalene as the oil phase. ME.0 and SE use histidine and ammonium phosphate buffers as their aqueous phase, respectively. The surfactants used in ME.0 and SE are PS 80 and a combination of 1, 2-dimyristoyl-sn-glycero-3-phosphocholine (DMPC) and Pluronic F68, respectively. In ME.0, sucrose is employed as an osmolyte, whereas glycerol is used in SE. SE also contains vitamin E which serves as an antioxidant and has also been shown to exert immunostimulatory activity.^{12; 13}

The protein antigen studied in this work is alpha toxin (AT) derived from *Staphylococcus aureus*. AT is one of the key virulent factors involved in *S. aureus* infection¹⁴ and has been found to be protective in animal models.¹⁵ AT is a promising vaccine candidate for protection against antibiotic resistant staphylococcus infection in high risk populations, especially patients hospitalized for surgery.⁷ The wild type AT is expressed by *S. aureus* extracellularly as a water soluble monomer and self-assembles into a homo-oligomeric heptamer with a transmembrane domain.¹⁶ The AT monomer consists of 293 amino acid with a molecular weight of 33.2 kDa. The AT used in this study is a mutant of the wild type AT which lacks the ability to self-assemble.

Emulsion adjuvants can be formulated with vaccine antigens in two different formats: single vial or separate vials in which antigen and adjuvant are mixed prior to administration.¹⁷ If antigen and adjuvant are compatible with each other, they can be formulated in a single vial to reduce manufacturing costs and provide ease of administration. Single vial formulation is therefore a more favorable option, especially as the commercial dosage form.² However, if antigens are not compatible with adjuvants over long-term storage, they must be stored separately before administration to ensure the safety and efficacy of a vaccine. This option is often implemented in early clinical trials when limited stability data are available. An understanding of emulsion/antigen interactions and how these interactions influence the

structure and stability of antigens is necessary to rationally decide the type of formulation (e.g. single vial or separate vial) and to further optimize the formulation to offer maximum antigen stability.^{18–20}

Since emulsions are usually optically turbid due to strong light scattering, this poses challenges for analytical characterization of antigens in their presence. Many routinely used spectroscopic techniques (such as Circular Dichroism (CD), UV absorption, and some forms of fluorescence) are often not suitable for this purpose because of the interference by light scattering.²¹ In the present study, a set of biophysical techniques capable of analyzing turbid protein samples were selected to investigate the secondary, tertiary structural integrity and overall conformation stability of protein antigens upon mixing with emulsion-based adjuvants. These techniques include Fourier transform infrared (FT-IR) and intrinsic fluorescence spectroscopy and differential scanning calorimetry (DSC).²² We have successfully used these techniques to characterize the effects of two oil-in-water (O/W) emulsion systems (designated as ME.0 and SE) on *Staphylococcal aureus* alpha toxin (AT), a potential vaccine antigen.

Materials and Methods

Materials

Frozen stock of recombinantly produced and purified AT in PBS buffer (pH 7.4) was obtained from Medimmune LLC (Gaithersburg, MD). The AT stock concentration was found to be 0.51 mg/ml (extinction coefficient, $A_{280\text{nm}}^{0.1\%} = 1.93$) by UV absorption spectroscopy and this value was used for sample preparation. Two oil-in-water emulsion-based adjuvants, ME.0 stock (2X) and SE stock (3X), were provided by MedImmune LLC (Gaithersburg, MD). ME.0 stock (2X) contains 20mM histidine at pH 6.0, 10% sucrose, 4% squalene and 1% PS80. SE stock (3X) is composed of 25mM ammonium phosphate, 5.1% squalene, 1.1% DMPC, 30ug/mL vitamin E, 2.37% w/v glycerol, and 0.037% w/v pluronic F68, at pH 5.6.

Sample preparation

ME.0 stock (2X) and SE stock (3X) were prepared by MedImmune LLC (Gaithersburg, MD) using a previously described protocol.² Briefly, squalene and surfactant were mixed and sonicated to achieve homogenous mixing of the oil phase. The aqueous phase was then added to the oil phase. The mixture was again homogenized using a Silverson L5M-A standard mixer (East Longmeadow, MA) and then subjected to microfluidization to generate milky emulsions of around 100 nm in size using a Microfluidics 110P microfluidizer (Microfluidics, Boston, MA). AT/ME.0 or AT/SE mixtures were prepared by mixing AT in PBS with an emulsion stock (ME.0 stock (2X) or SE stock (3X)) to achieve a final protein concentration of 0.2 mg/ml containing emulsion at 1X concentration.

In the component study, we aimed to study the effects of different emulsion components on AT (as per Table 1). AT was mixed with each water-soluble component of the emulsions at the same volumetric ratio as used in the AT/ME.0 or AT/SE mixture. S0 was prepared by diluting AT in PBS to achieve a concentration of 0.2 mg/ml. The compositions of all test

samples and their identification codes (M1 to M5 and S1 to S5) are listed in Table 1. For example, M1 was prepared by mixing AT in PBS (at 0.4 mg/mL) with 20 mM Histidine buffer, pH 6.0 at a volumetric ratio of 1:1. ME.0 (1X) and SE (1X) diluted using PBS were used as control samples. M2 was made by mixing AT in PBS (at 0.4 mg/mL) with a mixture solution containing 20 mM Histidine buffer (pH 6.0) and 10% sucrose at a volumetric ratio of 1:1. ME.0 (1X) and SE (1X) diluted using PBS were used as control samples. The mixtures were equilibrated at 4 °C overnight before analysis.

UV-visible absorption spectroscopy

The absorption spectrum of AT stock was collected using a UV/Visible spectrophotometer (Agilent Technologies, Santa Clara, CA) equipped with a diode array detector. The absorption spectra were corrected for scattering contributions by subtraction of an extrapolation of the logarithm of the optical density in a non-absorbing region (350 nm to 400 nm) to the far UV region.

FT-IR spectroscopy

FT-IR spectroscopic analysis was performed using a Tensor-27 FT-IR spectrometer (Bruker, Billerica, MA) equipped with a Bio-ATR cell. The detector was cooled with liquid N₂ for 20 min prior to use and the interferometer was purged continuously with N₂ gas. A total of 256 scans were recorded from 4000 to 900 cm⁻¹ with a 4 cm⁻¹ resolution. Buffer/emulsion background spectra were collected and subtracted from the sample spectra. Atmospheric compensation, baseline adjustment and second derivative calculations were applied using OPUS V6.5 (Bruker, Billerica, MA) software. To compare the initial state of the samples, spectra collected at 20 °C were deconvoluted into a set of mixed Gaussian/Lorentzian bands, using the build-in Levenberg-Maquardt algorithm from the OPUS V6.5 software. Thermal unfolding experiments were performed with the temperature ramped from 20 to 90 °C or 99 °C (for AT in SE) at increments of 2.5 °C per step and an equilibration time of 2 min at each temperature. The second derivative of each spectrum was calculated with nine point smoothing. The thermal unfolding curves of AT were constructed by plotting the second derivative signal at 1621 cm⁻¹ (an indication of intermolecular β -structure and protein aggregation) as a function of temperature. The melting temperature (T_m) was calculated by a first derivative method using Origin 2017 (OriginLab; Northampton, MA).

Intrinsic fluorescence spectroscopy

Intrinsic tryptophan fluorescence spectra were obtained using a fluorescence plate-reader (Fluorescence Innovations, Minneapolis, MN) equipped with a tunable pulsed dye laser, a high-speed digitizer and a temperature controlled 384-well sample holder (Torrey Pines Scientific, Carlsbad, CA). This fluorometer has two detectors: a charge coupled device (CCD) spectrometer and a photomultiplier tube (PMT), permitting recording of steady-state fluorescence and time-resolved intrinsic fluorescence, respectively. The emission signal was collected at 1803 (front face geometry) and then sent through a 300 nm long pass filter (Thorlabs Inc., Newton, NJ), which blocks the excitation light from entering the detector. For time-resolved fluorescence recording, the signal was further passed through a 360 nm (\pm 23 nm) band-pass filter before reaching the PMT. For steady-state fluorescence measurement, a right angle prism mirror was placed behind the 300 nm long pass filter to

direct the emission light through an optical fiber to the CCD detector. Samples were loaded into a 364 well plate (Hard-Shell 384-well PCR plates) and silicon oil (ThermoFisher Scientific, Waltham, MA) was added to avoid sample evaporation by covering the sample surface during temperature runs. Samples were excited at 295 nm (395% tryptophan emission). Temperature ramps were set from 20 to 99 °C with an increment of 1 °C per step and an equilibration time of 2 min at each temperature.

Steady-state emission spectra were collected using a CCD detector from 310 to 400 nm with an integration time of 100 ms. The mean center of spectra mass peak position (MSM peak position) and ratio of the area under the curve (AUC) from two regions (315 to 325 nm and 345 to 355 nm; $F_{345-355}/F_{315-325}$) were calculated using Matlab (MathWorks; Natick, MA). The MSM peak values are approximately 8 to 10 nm higher than the actual peak position but their use results in a better signal to noise ratio.²³

Time-resolved intrinsic fluorescence data was obtained by recording fluorescence lifetime decay waveforms within a time scale of 100 ns. Two parameters (sum and moment) were calculated from the raw waveform by the FII data analysis software (Fluorescence Innovations, Minneapolis, MN). Sum (in mV*ns) is the peak area under the waveform curve and represents the intensity of the overall emission collected by the PMT during an acquisition whereas moment (in ns) is defined as the center of the waveform where it equally divides the peak area under the curve. The moment represents the intensity-averaged lifetime of the waveform plot and its mathematical definition was previously described.^{24; 25} Those two parameters were plotted against temperature and a first derivative method was used to find the T_m employing Origin 7.0 (OriginLab; Northampton, MA).

Differential scanning calorimetry (DSC)

DSC was performed using a MicroCal VP-Capillary calorimeter (Malvern, UK) equipped with an autosampler. The temperature was ramped from 10 to 100 °C at a scan rate of 1 °C/min. The sample cell was equilibrated for 15 min at 10 °C at the beginning of each run using a filtering period of 16 sec. Samples were loaded into a 96-well plate. The plate was sealed and kept inside a sample container maintained at 5 °C. Apparent transition temperatures were calculated using a non-two-state equilibrium model in Origin 7.0 (OriginLab; Northampton, MA).

Dynamic light scattering (DLS) and zeta potential

DLS and zeta potential measurements were performed using a Zetasizer Nano ZS Helix (Malvern Instruments, Columbia, MD) equipped with a He-Ne laser 633nm and backscattering detection (173°). In the DLS experiment, emulsion samples were run without dilution because the hydrodynamic size of emulsions were previously found to be independent of dilution (up to 1000 fold).² Samples (50 µL) were loaded into a Helix micro cuvette (Malvern Instruments, Columbia, MD) with a Teflon stopper. Ten measurements were taken with an acquisition time of 10 sec per measurement. Samples were heated from 15 to 90 °C with a step of 2.5 °C and an equilibration time of 2 min at each step. The Z-average diameters were calculated for emulsion samples using a cumulant analysis. AT in PBS failed to produce consistent Z-average diameters due to its low molecular weight (33

kDa) and low concentration (0.2 mg/mL), therefore the derived count rate was reported instead. For the zeta potential measurement, samples were diluted two fold in water before analysis. Samples were measured in disposable folded capillary cells at 25 °C. The zeta-potential was calculated based on net electrophoretic mobility of sample particles using Henry's and the Smoluchowski approximations.

High-Performance Size-Exclusion Chromatography (HPSEC)

HPSEC analysis was performed using a Shimadzu HPLC system by measuring the fluorescence intensity at 330 nm upon excitation at 295nm. For HPSEC analysis, a TSKgel G3000SWXL column (7.8 mm × 300 mm) was used along with a TSKgel SWXL guard column (6.0 mm × 40 mm) from Tosoh Bioscience (King of Prussia, PA). A mobile phase composed of 0.2 M sodium phosphate, pH 6.8 was used. The concentrations of AT were maintained at 0.2 mg/mL by diluting with PBS, ME.0 or SE and 50 µL of sample was injected. The flow rate was 0.7 mL/min, and samples were held at 5°C in the auto sampler tray prior to injection.

Statistics

Statistical analyses between the control sample (i.e. AT in PBS or S0) and other test samples were performed using an independent two-sample t-test with equal variance. The variance equality was confirmed using the Levene's test. Values of $p < 0.05$ were considered to be statistically significant.

Results

FT-IR analysis of Recombinant AT with O/W Emulsions

The FTIR spectra in the Amide I region (1600–1700 cm^{-1}) of AT under various conditions and the corresponding deconvoluted spectra are shown in Figure 1 (panels A1 to A3). At 20 °C, in contrast to AT in PBS buffer, AT showed a statistically significant increase in alpha-helix content and decrease in beta-sheet content in the presence of SE rather than ME.0 (Figure 1, panel C1). Upon thermal stress, AT under all three conditions showed increases in the peak intensity at 1621 cm^{-1} corresponding to an increasing inter-molecular β -sheet content indicative of protein aggregation. This change is substantial for AT in PBS and in ME.0, but relatively minor for AT in SE (Figure 1, panels B1 to B3). Thermal unfolding profiles of AT monitored by the second derivative signal at 1621 cm^{-1} showed two transitions (Figure 1, panel C2). AT in PBS had two transitions at 56.6 ± 0.5 (T_{m1}) and 69.7 ± 0.5 (T_{m2}). In contrast to AT in PBS, AT in ME.0 showed slightly lowered T_{m1} values, but decreased T_{m2} values to a larger extent. SE significantly thermally stabilized AT as reflected by an increase of 15 °C and 22 °C in T_{m1} and T_{m2} values, respectively. The decreased extent of thermally induced protein aggregation observed for AT in SE can possibly be attributed to a stabilizing interaction between AT and SE.

Steady state intrinsic fluorescence spectroscopy analysis of recombinant AT with O/W Emulsions

Intrinsic fluorescence spectra of AT in PBS, ME.0 and SE at 20 °C were background subtracted and normalized for comparison. AT in PBS and in ME.0 shared similar emission

spectra with an emission λ_{\max} around 332 nm at 20 °C, suggesting the protein's overall tertiary structure was not significantly altered by the presence of ME.0. AT in SE, however, manifested a blue shifted spectrum with a λ_{\max} at 327 nm (Figure 2A) reflecting on average less exposure of the Trp residues to the aqueous environment. Since each AT molecule contains eight Trp residues, blue shifts are indicative of overall protein tertiary structure changes and may indicate hydrophobic interactions between AT and SE.

Both emulsions contains fluorescent components and shows significant fluorescence emission signals from 310 to 400 nm when excited at 295 nm. Thermal melting curves were plotted for both protein samples and emulsions to separately study their thermal transitions. ME.0 itself showed a thermal transition around 67 °C. SE, however, did not show a clear transition from 20 to 99 °C. Thermal unfolding profiles of AT in PBS showed only one thermal transition (Figure 2B and 2C). This transition was accompanied by a red shift in the MSM peak position and an increasing $F_{320-330}/F_{350-380}$ ratio, suggesting AT had a greater solvent exposure of tryptophan residues during thermal unfolding. AT in ME.0 showed combined transitions derived from AT and ME.0 (Figure 2B and 2C). The protein transition of AT in ME.0 showed similar changes (i.e. increasing MSM peak position and $F_{320-330}/F_{350-380}$ ratio) as seen in PBS. Conversely, AT in SE showed an opposite trend (i.e., a blue shift in MSM peak position and a decrease in $F_{320-330}/F_{350-380}$ ratio) during its thermal transition (Figure 2B and 2C). One possible explanation could be that AT interacted with SE during thermal unfolding with increasing exposure to the oil phase. Unfolding profiles monitored by both MSM peak position and $F_{320-330}/F_{350-380}$ ratio showed similar T_m values (Figure 2D). ME.0 slightly destabilized AT by a decrease of 4 – 5 °C in T_m , whereas SE enhanced the T_m of AT by approximately 12 °C.

Time-resolved intrinsic fluorescence analysis of Recombinant AT with O/W Emulsions

To tease out the effects of these complex O/W emulsions on AT protein stability, a component study was performed by studying the thermal stability of AT in the presence of water-soluble components using time-resolved intrinsic fluorescence spectroscopy. In the sum-temperature plot (Figure 3, panels A1 and A2), the decreasing trend line indicates thermal quenching of AT fluorescence. Moment is a lifetime-derived empirical parameter which reflects the overall polarity of the neighboring environment of tryptophan residues within a protein. AT in PBS (S0) monitored by both sum and moment showed one thermal transition (Figure 3, panels A1 and A2). The thermal transition exhibited an increase in the sum (collected at 360 nm) indicating an increasing population of exposed tryptophan residues in the protein during unfolding. An increase in the moment was observed for AT in PBS during thermal unfolding.

In contrast to S0, AT in M1 had a lower T_m by 4 °C probably because of a pH drop and/or change in salt composition after mixing AT in PBS (pH 7.4) with histidine buffer (20 mM, pH 6.0) (Figure 3, panel A3). Compared to M1, a minor drop in the T_m of AT was observed when mixed with 1% PS80 (M2), while adding 10 % sucrose (M3) slightly stabilized AT. Mixing both 1% PS80 and 10 % sucrose with AT (M4) showed effects by both of these two components (i.e., a thermally destabilizing and stabilizing effect from PS80 and sucrose, respectively). Compared to S0, AT in ME.0 (M5) produced decreased protein thermal

stability probably attributable to a change in the buffer composition upon mixing AT with ME.0.

In the component study of SE, AT mixed with water-soluble components of SE (samples referred to as S1 to S4) showed similar T_m values which were lower than that of S0. This suggests that ammonium phosphate (25 mM, pH 5.6) thermally destabilized AT, probably because of a drop in pH and/or change in salt composition. This effect was also observed for M1. In S4, because of the poor water solubility of DMPC, saturated DMPC aqueous solution was used and its concentration was lower than that used in SE (1.1%). It is possible that DMPC at the higher concentration present in SE may affect AT stability to a larger extent. AT in SE (S5), however, had a T_m as high as 71 °C (Figure 3B1 to B3). This dramatic thermal stabilization effect on AT is probably due to interactions between AT and the oil phase of SE consisting of squalene, vitamin E and DMPC (at 1.1%, a concentration higher than its aqueous solubility).

Differential scanning calorimetry analysis of recombinant AT with O/W Emulsions

DSC was performed to study the effect of emulsions on the overall conformational stability of AT. AT in PBS (S0) underwent two distinct thermal transitions ($T_{m1} = 58.0$ °C and $T_{m2} = 69.2$ °C, a relatively minor transition) (Figure 4A). The thermal unfolding of AT in PBS, ME.0 and SE was found to be irreversible as determined by rescanning the sample after one thermal unfolding cycle (data not shown). ME.0 showed two major transitions: the first one centered near 65.9 °C and the second one with a sudden large increase in heat capacity above 80 °C (see Supplementary Figure S1). The first transition, also seen by intrinsic fluorescence spectroscopy, may correspond to a structural change in the emulsion, while the second one probably reflects the complete decomposition of the emulsion system. The AT/ME.0 mixture (M5) exhibited transitions from both protein and emulsion with the second thermal transition of AT and that of ME.0 partially overlapped. ME.0 lowered both T_{m1} and T_{m2} of AT significantly (compare samples M5 vs. S0 in Figure 4A). On the other hand, the T_m of ME.0 decreased by 3.5 °C in the presence of AT indicating that partially unfolded AT may slightly destabilize ME.0. For the component study, DSC was performed to study the effects of various components on the T_m of AT. Each component showed a similar effect on melting temperatures (T_{m1} and T_{m2}) of AT as indicated by the lifetime fluorescence component study (Figure 4AM1 to M4). This result further suggests that the destabilization effect of ME.0 on AT is because of the change in buffer composition upon mixing.

In the range of 10 to 100 °C, SE showed one thermal transition around 25.3 °C, corresponding to a gel-liquid phase transition of DMPC²⁶ (Figure 4B and Supplementary Figure S1). This result was further confirmed by examining saturated DMPC solution in 25 mM ammonium phosphate (the concentration of DMPC is less than 1.1%) by DSC which showed a transition at 24.6 °C (Figure 4B). Upon mixing AT with SE (S5), the T_m of SE was not significantly altered by AT. SE, however, increased both T_{m1} and T_{m2} of AT by 13.7 and 25.9 °C, respectively (compare samples S5 vs. S1 in Figure 4B). The component study was continued by mixing AT with the water-soluble components present in SE. The DSC results correlate well with the intrinsic fluorescence data. It shows that the change in buffer

composition upon mixing (S1) induced a destabilization effect on AT thermal stability while neither 2.37% glycerol (S3) nor 0.037% F68 (S2) had a further significant effect on the T_m of AT. Mixing saturated DMPC (S4) with AT produced only a minor increase in protein T_{m1} and T_{m2} . Overall, all of water soluble components of SE did not show a major stabilization effect on AT T_m . The dramatic stabilization effect of SE (S5) on AT is therefore probably due to the interaction between AT and the oil phase containing squalene, vitamin E and DMPC (at 1.1%).

Dynamic light scattering (DLS) and zeta potential analysis of recombinant AT with O/W Emulsions

DLS was performed to investigate the effect of temperature on the colloidal stability of the samples. As shown in Figure 5A, the derived count rate (i.e. the intensity of light scattering) of AT in PBS showed a dramatic increase above 52.5 °C, indicating the aggregation of AT in PBS. This result is in good agreement with the stability data reported above. SE did not show dramatic changes in their hydrodynamic sizes between 15 and 90 °C, suggesting the high colloidal stability of SE upon thermal stress (Figure 5B). The size of SE above 90 °C was not measured because of instrumental constraint. The addition of AT to SE did not change the overall size of emulsion nanoparticles. In addition, the first unfolding event of AT (around 70 °C seen by DSC etc.) did not significantly alter the emulsion size. In contrast, heating caused ME.0 to aggregate above 60 °C (Figure 5C). The addition of AT into ME.0 further decreased the onset aggregation temperature by approximately 3 °C, which is consistent with the DSC data. Zeta potential analysis shows that AT had a slight negative zeta potential at pH 7.4 due to its pI value (~ 6.85) (Figure S2). Both ME.0 and AT in ME.0 had a slightly negative zeta potential, presumably due to negatively charged impurities (such as free fatty acids²⁷) in PS80. In contrast, SE showed a neutral zeta potential. AT in SE also showed a near zero potential probably because the mixing AT (pH 7.4) with SE (pH 5.6) results in a mixture with a pH closer to the pI of AT.

High-Performance size-exclusion chromatography (HPSEC) analysis of recombinant AT with O/W Emulsions

SEC was performed to study the impact of the interactions of AT and ME.0/SE on retention time of the protein and the individual emulsions. Figure 6 shows the SEC chromatograms for AT in PBS, and when mixed with ME and SE. AT has a single peak eluting at ~16.9 min (Fig. 6A). Both ME.0 and SE elute at 8 to 9 min (Figure 6A and 6B). When mixed with ME.0, the retention time of AT does not change significantly and the recovery of AT was found to be 99.7 ± 0.1 % (Supplementary Table S1). When AT is mixed with SE, the peak corresponding to AT is missing while the peak at 9 min had a larger peak area than the peak area of SE alone (Figure 6B). This result may indicate that the AT is bound to the SE and co-elutes with the emulsion.

Discussion

In the present study, the effects of two squalene based emulsion adjuvants (ME.0 and SE) on the structure and stability of recombinant AT, a potential vaccine candidate for antibiotic resistant *Staph* infection, were investigated. The wild type AT is expressed as water soluble

monomer and self-assembles into a heptameric structure with a transmembrane domain.¹⁶ AT used in this study is a mutant of the wild type AT and may still have favorable interactions with phospholipid bilayers (i.e. DMPC) and/or the hydrophobic oil phase in the emulsion adjuvants. FT-IR, intrinsic tryptophan fluorescence, DSC and DLS were performed to investigate protein structure and the thermal stability of AT in the presence of emulsions. These results are summarized in Table 2. FTIR spectra of AT at 20 °C indicate that AT had an increased alpha helix content, but decreased the amount of beta sheet in the presence of SE. This effect on AT is negligible for ME.0, but more pronounced in the presence of SE. Previous work has reported that protein/oil interactions induced a protein to undergo a transition from beta sheet to more non-native alpha helix content in a β -lactoglobulin/hexadecane system.²⁸ At 20 °C, a significant blue shift (λ_{max} changed from 332 to 327 nm) was observed in the intrinsic fluorescence emission spectrum of AT in SE, rather than AT in ME.0. This result correlates with FTIR data indicating that SE but not ME.0 induced substantial structural alterations of AT in SE.

Protein thermal stability analysis shows that ME.0 slightly decreased the T_m of AT, while it was significantly enhanced in the presence of SE. A component study was further conducted by characterizing AT in the presence of the individual water-soluble components of the test emulsions with the goal of identifying the components responsible for alterations of protein stability. The data shows that the destabilizing impact of ME.0 on AT is probably because of a change in the buffer composition upon mixing ME.0 which contains 20 mM histidine (pH 6.0) with AT in PBS (pH 7.4). In the case of AT in SE, because none of the water soluble components produced a thermal stabilization effect on AT, it seems probable that the thermal stabilization of SE is due to interactions between AT and the oil phase of SE consisting of squalene, vitamin E and DMPC.

SE significantly altered the secondary and tertiary structures of AT and improved its thermal stability. This was again probably because of the adsorption of AT onto the oil phase. Proteins at oil-water interfaces have previously shown enhanced resistance to thermal stress.²⁸ Zhai has reported no significant changes in the secondary structure of β -lactoglobulin adsorbed to nonpolar hexadecane up to 76 °C at which point the same protein in solution lost its secondary structure.²⁸ When protein molecules interact with hydrophobic oil, they usually tend to reorient their apolar patches towards the oil surface to enhance apolar interactions. This is usually accompanied by structural changes in proteins. In this case, an interconversion from beta sheet to alpha helix was observed for AT in the presence of SE. Upon adsorption to SE, AT showed less exposure of Trp residues to the polar environment and an increased thermal stability. DLS analysis indicates that SE exhibited higher colloidal stability than ME.0 in response to heating. The addition of AT decreased the stability of ME.0 but did not impact SE (at least up to 90 °C). The zeta potential data show that SE had a relatively neutral surface, suggesting that the ionic attraction between SE and AT is probably negligible, further arguing that the potential interaction is hydrophobically driven. In addition, HPSEC data showed a nearly complete loss in the recovery of AT when mixed with SE, but not ME.0, indicating a high degree of interaction with SE, which possibly resulted in the co-elution of AT with SE.

Both ME.0 and SE are squalene based oil-in-water emulsions, but they interact with AT quite differently. They mainly differ in the type and concentration of surfactants. This might be responsible for the difference in their effects on protein structure and stability. In a stable emulsion system, oil droplets are coated by stabilizing surfactants. Protein molecules need to displace surfactant to adsorb onto the surface of an oil phase. In the case of ME.0, AT probably failed to compete with polysorbate 80 (at 0.5%) for binding to the surface of oil droplets. On the other hand, AT probably was better able to displace the surfactants of SE (DMPC and pluronic F68) to establish interactions with its oil phase. It is also possible that AT interact with the lipid layer of DMPC at the concentration of 1.1% used in SE, which is significantly higher than its aqueous solubility. It is worthwhile mentioning that during the unfolding of AT, the emulsions had undergone (SE) or were undergoing (ME.0) thermal transitions (Figure 4). It is possible that emulsion structural changes contribute to the observed changes in protein thermal stability.

FTIR, intrinsic fluorescence spectroscopy and DSC have shown significant robustness in characterizing the structure and conformational stability of alpha-toxin (AT), a vaccine candidate for *Staph* infection, in the presence of highly scattering squalene based emulsion adjuvants. The component study further helped to dissect the effect of each water soluble component on the protein antigen. These biophysical methods along with the component study can be considered a case study to be applied to study the structure and stability of other protein antigens in a variety of adjuvant emulsion systems, further guiding the development and optimization of emulsion-adjuvanted vaccine formulations.

Supplementary Material

Refer to Web version on PubMed Central for supplementary material.

Acknowledgments

The KU authors wish to acknowledge MedImmune for providing financial support and the experimental materials, the NIH biotechnology training grant (5T32GM008359-26) to Nicholas Larson. We would like to thank Malvern Panalytical for providing the Zetasizer Nano ZS Helix instrument.

References

1. Moyle PM, Toth I. Modern subunit vaccines: Development, components, and research opportunities. *ChemMedChem*. 2013; 8(3):360–376. [PubMed: 23316023]
2. Iyer V, Cayatte C, Marshall JD, Sun J, Schneider-Ohrum K, Maynard SK, Rajani GM, Bennett AS, Remmele RL, Bishop SM. Feasibility of freeze-drying oil-in-water emulsion adjuvants and subunit proteins to enable single-vial vaccine drug products. *J Pharm Sci*. 2017; 106(6):1490–1498. [PubMed: 28259764]
3. Leroux-Roels G. Unmet needs in modern vaccinology: Adjuvants to improve the immune response. *Vaccine*. 2010; 28:C25–C36. [PubMed: 20713254]
4. Garcon N, Vaughn DW, Didierlaurent AM. Development and evaluation of as03, an adjuvant system containing α -tocopherol and squalene in an oil-in-water emulsion. *Expert review of vaccines*. 2012; 11(3):349–366. [PubMed: 22380826]
5. Ott G, Barchfeld GL, Chernoff D, Radhakrishnan R, van Hoogevest P, Van Nest G. Vaccine design. Springer; 1995. Mf59 design and evaluation of a safe and potent adjuvant for human vaccines; 277–296.

6. Podda A, Del Giudice G. Mf59-adjuvanted vaccines: Increased immunogenicity with an optimal safety profile. *Expert review of vaccines*. 2003; 2(2):197–204. [PubMed: 12899571]
7. Jackson LA, Campbell JD, Frey SE, Edwards KM, Keitel WA, Kotloff KL, Berry AA, Graham I, Atmar RL, Creech CB. Effect of varying doses of a monovalent h7n9 influenza vaccine with and without as03 and mf59 adjuvants on immune response: A randomized clinical trial. *Jama*. 2015; 314(3):237–246. [PubMed: 26197184]
8. Reed SG, Orr MT, Fox CB. Key roles of adjuvants in modern vaccines. *Nature medicine*. 2013; 19(12):1597–1608.
9. O'Hagan D, Ott G, De Gregorio E, Seubert A. The mechanism of action of mf59—an innately attractive adjuvant formulation. *Vaccine*. 2012; 30(29):4341–4348. [PubMed: 22682289]
10. Behzad H, Huckriede AL, Haynes L, Gentleman B, Coyle K, Wilschut JC, Kollmann TR, Reed SG, McElhaney JE. GlA-se, a synthetic toll-like receptor 4 agonist, enhances t-cell responses to influenza vaccine in older adults. *J Infect Dis*. 2011; 205(3):466–473. [PubMed: 22147791]
11. Sun J, Remmele RL, Sanyal G. Analytical characterization of an oil-in-water adjuvant emulsion. *AAPS PharmSciTech*. 2016:1–10.
12. Wu D, Meydani SN. Age-associated changes in immune and inflammatory responses: Impact of vitamin e intervention. *J Leukocyte Biol*. 2008; 84(4):900–914. [PubMed: 18596135]
13. Morel S, Didierlaurent A, Bourguignon P, Delhay S, Baras B, Jacob V, Planty C, Elouahabi A, Harvengt P, Carlsen H. Adjuvant system as03 containing α -tocopherol modulates innate immune response and leads to improved adaptive immunity. *Vaccine*. 2011; 29(13):2461–2473. [PubMed: 21256188]
14. Wardenburg JB, Bae T, Otto M, DeLeo FR, Schneewind O. Poring over pores: A-hemolysin and panton-valentine leukocidin in staphylococcus aureus pneumonia. *Nature medicine*. 2007; 13(12):1405–1406.
15. Adhikari RP, Karauzum H, Sarwar J, Abaandou L, Mahmoudieh M, Boroun AR, Vu H, Nguyen T, Devi VS, Shulenin S. Novel structurally designed vaccine for s. Aureus α -hemolysin: Protection against bacteremia and pneumonia. *PLoS One*. 2012; 7(6):e38567. [PubMed: 22701668]
16. Song L, Hobaugh MR, Shustak C, Cheley S, Bayley H, Gouaux JE. Structure of staphylococcal alpha-hemolysin, a heptameric transmembrane pore. *Science*. 1996; 274(5294):1859–1866. [PubMed: 8943190]
17. Ott G, Radhakrishnan R, Fang J-H, Hora M. The adjuvant mf59: A 10-year perspective. Springer; 2000. 211–228.
18. Fox CB, Kramer RM, Barnes VL, Dowling QM, Vedvick TS. Working together: Interactions between vaccine antigens and adjuvants. *Therapeutic advances in vaccines*. 2013; 1(1):7–20. [PubMed: 24757512]
19. Dey AK, Malyala P, Singh M. Physicochemical and functional characterization of vaccine antigens and adjuvants. *Expert review of vaccines*. 2014; 13(5):671–685. [PubMed: 24702271]
20. Kumru OS, Joshi SB, Smith DE, Middaugh CR, Prusik T, Volkin DB. Vaccine instability in the cold chain: Mechanisms, analysis and formulation strategies. *Biologicals*. 2014; 42(5):237–259. [PubMed: 24996452]
21. Ji T, Urry D. Correlation of light scattering and absorption flattening effects with distortions in the circular dichroism patterns of mitochondrial membrane fragments. *Biochemical and biophysical research communications*. 1969; 34(4):404–411. [PubMed: 5776388]
22. li Zhai J, Day L, Aguilar M-I, Wooster TJ. Protein folding at emulsion oil/water interfaces. *Current opinion in colloid & interface science*. 2013; 18(4):257–271.
23. Hu L, Joshi SB, Andra KK, Thakkar SV, Volkin DB, Bann JG, Middaugh CR. Comparison of the structural stability and dynamic properties of recombinant anthrax protective antigen and its 2-fluorohistidine-labeled analogue. *J Pharm Sci*. 2012; 101(11):4118–4128. [PubMed: 22911632]
24. Petersen KJ, Peterson KC, Muretta JM, Higgins SE, Gillispie GD, Thomas DD. Fluorescence lifetime plate reader: Resolution and precision meet high-throughput. *Rev Sci Instrum*. 2014; 85(11):113101. [PubMed: 25430092]
25. Wei Y, Larson NR, Angalakurt SK, Middaugh CR. Improved fluorescence methods for high-throughput protein formulation screening. *SLAS TECHNOLOGY*. 2018 (in press).

26. Gilman T, Kauffman JW, Pownall HJ. Raman spectroscopy of the thermal properties of reassembled high-density lipoprotein: Apolipoprotein ai complexes of dimyristoylphosphatidylcholine. *Biochemistry*. 1981; 20(3):656–661. [PubMed: 6783071]
27. Brandner JD. The composition of nf-defined emulsifiers: Sorbitan monolaurate, monopalmitate, monostearate, monooleate, polysorbate 20, polysorbate 40, polysorbate 60, and polysorbate 80. *Drug Dev Ind Pharm*. 1998; 24(11):1049–1054. [PubMed: 9876559]
28. Zhai J, Wooster TJ, Hoffmann SV, Lee T-H, Augustin MA, Aguilar M-I. Structural rearrangement of β -lactoglobulin at different oil–water interfaces and its effect on emulsion stability. *Langmuir*. 2011; 27(15):9227–9236. [PubMed: 21668007]

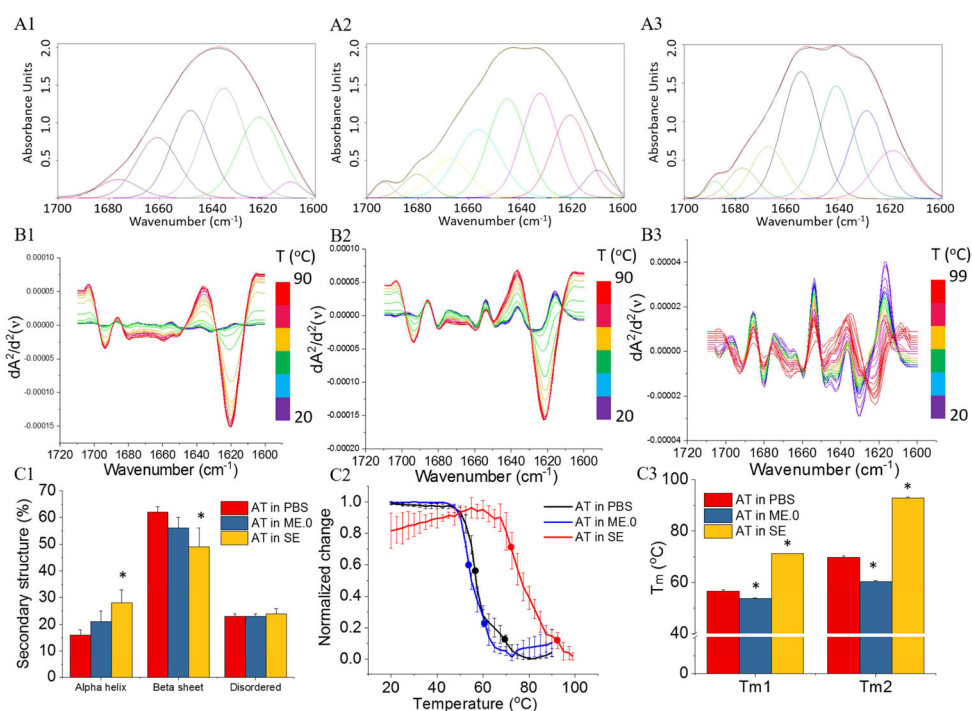


Figure 1.

Structure and stability of AT in presence and absence of ME.0 and SE emulsions as measured by FTIR. FTIR spectra of (A1) AT in PBS at 20 °C; (A2) AT with ME.0 at 20 °C; (A3) AT with SE at 20 °C. The black and red lines represent the raw and fitted FTIR spectra, respectively. The deconvoluted spectra are shown in various colors. Spectra with peaks between 1649–1659 cm⁻¹ are assigned as α helix; spectra with peaks between 1620–1640 cm⁻¹ or 1661–1700 cm⁻¹ are assigned as β sheet. Other peaks are assigned as disordered. Second derivative of FTIR spectra monitoring the thermal unfolding of (B1) AT in PBS from 20 to 90 °C; (B2) AT with ME.0 from 20 °C to 90 °C; (A3) AT with SE from 20 °C to 99 °C. (C1) The secondary structural contents of AT determined by deconvolution analysis. AT in SE, but not AT in ME.0, showed a statistically significant difference with AT in PBS in protein secondary structure contents. * $p < 0.05$. (C2) Thermal melting curve of AT monitored by changes in the signal at 1621 cm⁻¹. Round dots on each melting curves indicate melting temperatures. (C3) Comparison of thermal melting temperature values of AT under various conditions (N = 3). * $p < 0.05$.

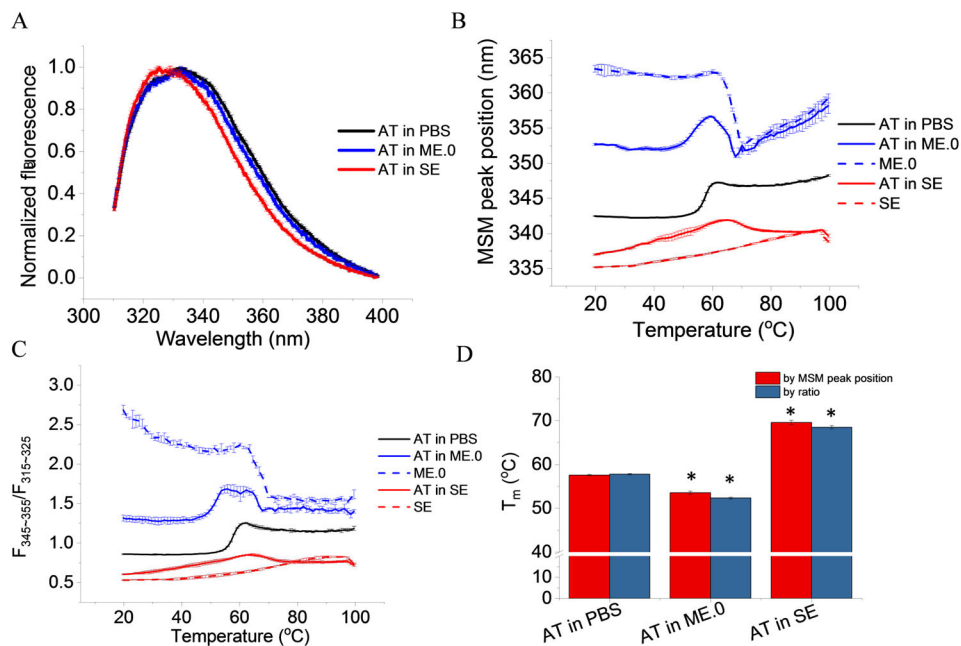


Figure 2. Tertiary structure analysis of AT in presence and absence of ME.0 and SE emulsions as monitored by intrinsic fluorescence spectroscopy. (A) Normalized fluorescence spectra of AT at 20 °C. Thermal unfolding profiles monitored by (B) MSM peak position and (C) ratio of the area under the curve (AUC) from two regions ($F_{320-330}/F_{350-380}$) (E) Summary of T_m values. Error bars indicate standard deviation ($N=3$). * $p < 0.05$.

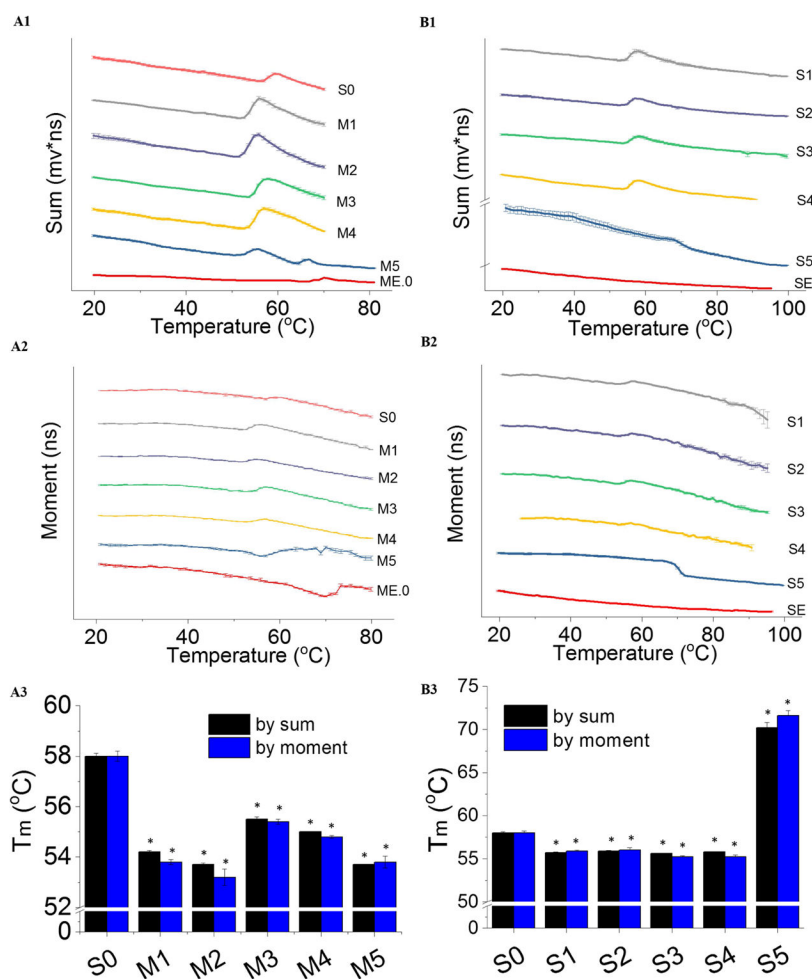
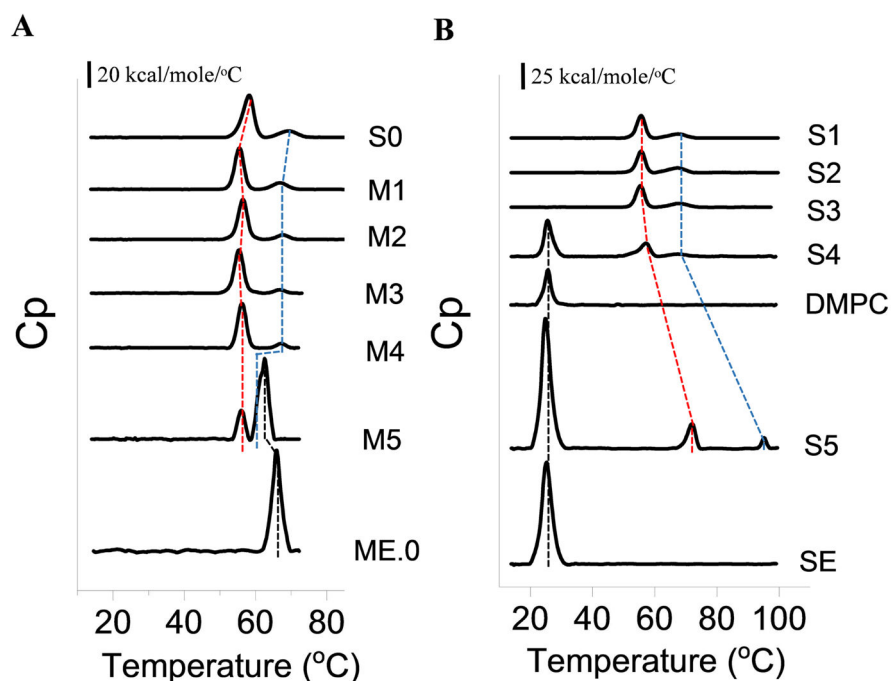


Figure 3. Thermal unfolding profiles of AT in the presence of various components of ME.0 emulsion as measured by time resolved fluorescence spectroscopy. The sum (A1) and moment (A2) values of AT emission waveforms; of SE monitored by sum (B1) and moment (B2) of AT emission waveforms. Corresponding T_m values are summarized (panels A3 and B3). Error bar indicates standard deviation (N=3). * $p < 0.05$. See Table 1 for sample composition.



Samples	S0	M1	M2	M3	M4	M5	S1	S2	S3	S4	S5
$T_{m1}(^{\circ}\text{C})$	58.0 ± 0.02	55.4 ± 0.02 *	55.3 ± 0.03 *	56.4 ± 0.04 *	56.2 ± 0.02 *	56.0 ± 0.05 *	55.5 ± 0.03 *	55.5 ± 0.01 *	55.3 ± 0.02 *	56.7 ± 0.23 *	71.7 ± 0.07 *
$T_{m2}(^{\circ}\text{C})$	69.2 ± 0.16	66.9 ± 0.16 *	66.8 ± 0.04 *	67.7 ± 0.07 *	67.2 ± 0.03 *	60.8 ± 0.37 *	67.3 ± 0.17 *	67.0 ± 0.12 *	67.8 ± 0.27 *	67.9 ± 0.61 *	95.1 ± 0.06 *

Figure 4.

DSC thermograms of AT, emulsions, and AT in the presence of various components of emulsions (A) ME.0 and (B) SE. The first (T_{m1}) and second (T_{m2}) thermal transitions of AT are indicated by red and blue dashed lines, respectively. The transition derived from emulsions (ME.0 and SE) is indicated using black dashed line. Apparent melting temperature values are summarized in the table. Errors indicate standard deviation (N=3). See Table 1 for sample composition. * $p < 0.05$.

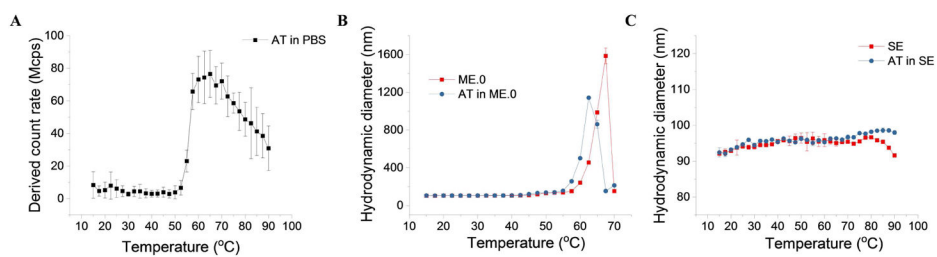


Figure 5. The temperature dependent colloidal stability of AT in PBS (A), AT in ME.0 (B), and AT in SE (C) measured by dynamic light scattering. Errors indicate standard deviation (N=3). See Table 1 for sample composition.

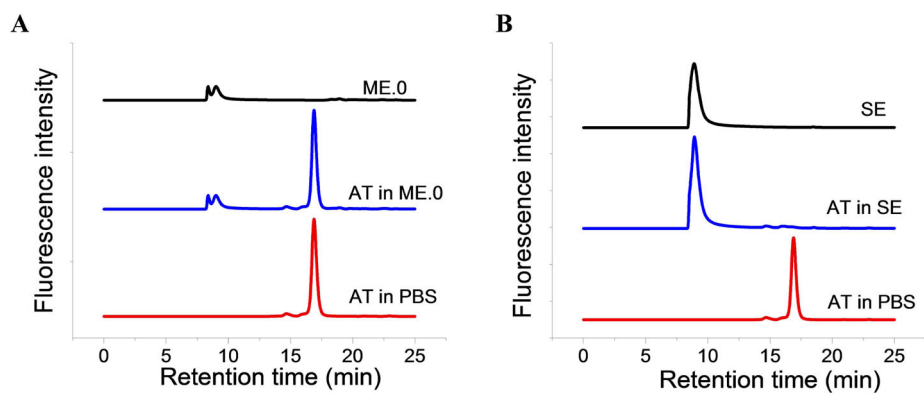


Figure 6. HPSEC chromatograms of ME.0 and AT in ME.0 (A); SE and AT in SE (B). The chromatography of AT in PBS was shown in both plots for comparison.

Identification codes and components of test samples subjected to the component study. All test samples used for the component study contained AT with a concentration of 0.2 mg/ml. S0 is AT in PBS (at 0.2 mg/ml), ME.0 (1X) and SE (1X) diluted using PBS were used as control samples. S0, M5 and S5 are denoted as AT in PBS, AT in ME.0 and AT in SE, respectively in FTIR, steady-state fluorescence, and HPSEC studies. * For S4, AT was mixed with saturated aqueous solution of DMPC with a concentration lower than 1.1% used in SE.

Table 1

S0	AT in PBS (at 0.2 mg/mL)					
	ME.0 component study samples	20mM Histidine pH 6.0	AT in PBS (0.4 mg/ml) mixed with (1/1, v/v)	10% Sucrose	1% PS80	4% Squalene
M1		+				
M2		+		+		
M3		+			+	
M4		+		+	+	
M5		+		+	+	+
SE component study samples	AT in PBS (0.3 mg/ml) mixed with (2/1, v/v)					
	25mM Ammonium Phosphate pH 5.6 <th>Pluronic F68 0.037% (w/v)</th> <th>Glycerol 2.37% (w/v)</th> <th>DMPC 1.1%</th> <th>5.1% Squalene 30 µg/mL Vitamin E</th>	Pluronic F68 0.037% (w/v)	Glycerol 2.37% (w/v)	DMPC 1.1%	5.1% Squalene 30 µg/mL Vitamin E	
S1	+					
S2	+	+				
S3	+		+			
S4	+			+	+	
S5	+	+	+	+	+	

Table 2

Summary of biophysical data sets of AT in ME.0 or SE compared to AT in buffer alone. The biophysical techniques used in this study and corresponding parameters investigated are listed. The relative change in these parameters for AT in ME.0 or SE relative to AT in PBS.

Technique	Biophysical parameter studied	AT in ME.0	AT in SE	
FT-IR	2 nd structure content at 20 °C	α -helix	↑ 5%	↑ 12% @ 20 °C
		β -sheet	↓ 6%	↓13% @ 20 °C
		random coil	no change	no change
	T_{m1}	↓ 2.9 °C	↑ 14.6 °C	
	T_{m2}	↓ 9.3 °C	↑ 23.2 °C	
Steady-state fluorescence	T_m by MSM peak position	↓ 4.0 °C	↑ 12.0 °C	
	T_m by ratio	↓ 5.4 °C	↑ 10.7 °C	
Time resolved fluorescence	T_m by moment	↓ 4.2 °C	↑ 12.2 °C	
	T_m by sum	↓ 4.3 °C	↑ 13.6 °C	
DSC	T_{m1}	↓ 2.0 °C	↑ 13.7 °C	
	T_{m2}	↓ 8.4°C	↑ 25.9 °C	
SEC	Recovery of AT		~ 0%	